The Xist lncRNA Exploits Three-Dimensional Genome Architecture to Spread Across the X Chromosome

Citation: Engreitz, J. M., A. Pandya-Jones, P. McDonel, A. Shishkin, K. Sirokman, C. Surka, S. Kadri, et al. "The Xist lncRNA Exploits Three-Dimensional Genome Architecture to Spread Across the X Chromosome." Science 341, no. 6147 (August 16, 2013): 1237973–1237973.

As Published: http://dx.doi.org/10.1126/science.1237973

Publisher: American Association for the Advancement of Science (AAAS)

Persistent URL: http://hdl.handle.net/1721.1/85575

Version: Author's final manuscript: final author's manuscript post peer review, without publisher's formatting or copy editing

Published in final edited form as:
Science. 2013 August 16; 341(6147): 1237973. doi:10.1126/science.1237973.

The Xist lncRNA exploits three-dimensional genome architecture to spread across the X-chromosome*

Jesse M. Engreitz[1,2], **Amy Pandya-Jones**[3], **Patrick McDonel**[1], **Alexander Shishkin**[1], **Klara Sirokman**[1], **Christine Surka**[1], **Sabah Kadri**[1], **Jeffrey Xing**[1], **Alon Goren**[1], **Eric S. Lander**[1,4,5,*,†], **Kathrin Plath**[3,*,†], and **Mitchell Guttman**[1,*,†,‡]

[1]Broad Institute of Harvard and MIT, Cambridge MA 02142

[2]Division of Health Sciences and Technology, MIT, Cambridge MA 02139

[3]Department of Biological Chemistry, Jonsson Comprehensive Cancer Center, Molecular Biology Institute, and Eli and Edythe Broad Center of Regenerative Medicine and Stem Cell Research, David Geffen School of Medicine, University of California Los Angeles, Los Angeles, CA 90095

[4]Department of Biology, MIT, Cambridge MA 02139

[5]Department of Systems Biology, Harvard Medical School, Boston MA 02114

Abstract

Many large noncoding RNAs (lncRNAs) regulate chromatin, but the mechanisms by which they localize to genomic targets remain unexplored. Here we investigate the localization mechanisms of the Xist lncRNA during X-chromosome inactivation (XCI), a paradigm of lncRNA-mediated chromatin regulation. During the maintenance of XCI, Xist binds broadly across the X-chromosome. During initiation of XCI, Xist initially transfers to distal regions across the X-chromosome that are not defined by specific sequences. Instead, Xist identifies these regions by exploiting the three-dimensional conformation of the X-chromosome. Xist requires its silencing domain to spread across actively transcribed regions and thereby access the entire chromosome. This suggests a model where Xist coats the X-chromosome by searching in three dimensions, modifying chromosome structure, and spreading to newly accessible locations.

Introduction

Mammalian genomes encode thousands of large non-coding RNAs (lncRNAs) (1-5), many of which play key functional roles in the cell (6-9). One emerging paradigm is that many lncRNAs can regulate gene expression (6, 8-11) by interacting with chromatin regulatory complexes (6, 12-14) and localizing these complexes to genomic target sites (15-17). Despite the central role of RNA-chromatin interactions, the mechanisms by which lncRNAs identify their genomic targets remain unexplored.

The Xist ncRNA provides a model to investigate the mechanisms of lncRNA localization (11, 18, 19). Xist initiates X-chromosome inactivation (XCI) by spreading in *cis* across the future inactive X-chromosome (20, 21), recruiting the polycomb repressive complex 2

*Correspondence to: mguttman@caltech.edu, KPlath@mednet.ucla.edu, or lander@broadinstitute.org.
†These authors contributed equally to this work.
‡Current address: Division of Biology, California Institute of Technology, Pasadena, CA

(PRC2) (14, 22, 23), and forming a transcriptionally silent nuclear compartment (24, 25) enriched for repressive chromatin modifications including H3K27me3 (22, 23). These functions of Xist – localization to chromatin and silencing of gene expression – are mediated by distinct RNA domains (26): transcriptional silencing requires the A-repeat domain (26), which interacts with the PRC2 chromatin regulatory complex (14), while localization to chromatin requires several distinct domains (26-28) and interactions with proteins associated with the nuclear matrix (29-31). Despite these advances in our understanding of Xist, we still do not understand the process by which Xist localizes to chromatin and spreads across the X-chromosome.

Here we present a biochemical method that enables high-resolution mapping of lncRNA localization. Using this method, we explored Xist localization during initiation and maintenance of XCI. During maintenance, Xist localized broadly across the entire X-chromosome, lacking focal binding sites. During initiation of XCI, Xist transferred directly from its transcription locus to distal sites across the X-chromosome that are defined not by specific sequences but by their spatial proximity in the nucleus to the Xist transcription locus. Furthermore, we show that Xist initially localized to the periphery of actively transcribed regions, but gradually spread across them through a mechanism dependent on the A-repeat domain. Together, these results suggest that Xist initially localizes to distal sites across the chromosome by exploiting chromosome conformation, and may spread to new sites through its ability to modify chromatin structure.

Results and Discussion

RNA Antisense Purification (RAP): A method to map lncRNA interactions with chromatin

To determine the genomic localization of lncRNAs, we developed a method termed RNA Antisense Purification (RAP), which is conceptually similar to previous methods (32-34) in that it uses biotinylated antisense probes that hybridize to a target RNA to purify the endogenous RNA and its associated genomic DNA from crosslinked cell lysate (Fig. 1A) (35). We designed RAP to enable specific purification of chromatin associated with a target lncRNA, achieve high resolution mapping of the associated DNA target sites upon sequencing of the captured DNA, and robustly capture any lncRNA with minimal optimization. To achieve high specificity, RAP utilizes 120-nucleotide antisense RNA probes in order to form extremely strong hybrids with the target RNA thereby enabling purification using denaturing conditions that disrupt nonspecific RNA-protein interactions and nonspecific hybridization with RNAs or genomic DNA. To achieve high resolution, RAP uses DNase I to digest genomic DNA to ~150bp fragments, which provides high resolution mapping of binding sites. To robustly capture a lncRNA, RAP uses a pool of overlapping probes tiled across the entire length of the target RNA to ensure capture even in the case of extensive protein-RNA interactions, RNA secondary structure, or partial RNA degradation (supplementary online text).

To test our method, we used RAP to purify the Xist RNA and associated DNA from female mouse lung fibroblasts (MLFs), a differentiated cell line in which Xist is expressed from and coats the inactive X-chromosome. We designed antisense probes tiled every 15 nucleotides across the 17-Kb Xist transcript, excluding those that showed any complementarity to other RNAs or genomic DNA regions (35). This yielded a pool of 1,054 unique probes. We performed RAP and observed a >100-fold enrichment of the Xist RNA compared to either input or a control purification using ‘sense’ probes from the same strand as Xist itself (Fig. 1B). When we sequenced all RNAs in the purified fraction, we found that the Xist RNA comprised ~70% of alignable reads despite representing <0.1% of the polyadenylated input RNA. The remaining reads were broadly distributed across ~7,500 expressed transcripts, with no single transcript exceeding 2% of the total purified RNA (Fig. 1C). We sequenced

the genomic DNA that co-purified with the Xist RNA and observed a strong enrichment with >70% of the DNA sequencing reads from the Xist purification originating from the X-chromosome, compared to ~5% from the input DNA samples (Fig. 1D).

To ensure that the DNA purified by Xist RAP reflected the endogenous localization of Xist, we performed three controls (Fig. S1) (35). (i) To confirm that captured chromatin reflected pre-existing interactions occurring *in vivo*, we purified Xist from non-crosslinked cellular extracts. In this condition, we did not obtain any detectable DNA signal by qPCR despite obtaining comparable enrichments of the Xist RNA (35). (ii) To rule out the possibility that RAP captured genomic DNA through nonspecific hybridization with the probes or the target RNA, we tested whether sites with higher enrichment in Xist RAP showed complementarity to sequences present in the probes or Xist RNA sequence (35). We observed no relationship between sequence homology and RNA localization either on the X-chromosome or on autosomes (Fig. S2). (iii) To further exclude the possibility of direct probe-DNA interactions, we examined DNA captured in a control purification with sense probes which should capture double-stranded DNA with the same efficiency, but will not hybridize to the target RNA. Using the sense probes, we observed no enriched regions across the entire genome (Fig. 1D) with the sole exception of a low-level enrichment at the *Xist* locus itself (35), likely reflecting perfect hybridization with the RNA probes. Yet, the amount of Xist genomic DNA purified in the control was <5% of the amount in the Xist purification, suggesting that most of the signal in Xist RAP resulted from RNA-mediated interactions (supplemental online text).

Together, these results demonstrate the specificity of the RAP method to capture RNA interactions with chromatin.

Xist binds across the inactive X in differentiated female cells

Using RAP, we explored the localization of Xist in MLFs. We found that Xist showed enrichment over the entire X-chromosome as opposed to showing punctate enrichment at specific locations (Fig. 2A-C, Fig. S3). Indeed, >95% of 10-Kb windows on the X-chromosome were enriched more than 10-fold compared to the input. In comparison, not a single window on an autosome reached this enrichment level (Fig. 2C). This broad localization pattern contrasts sharply with the roX2 ncRNA in *Drosophila*, which, despite its similar function of regulating gene expression across an entire chromosome, binds at discrete sites (32, 33).

While Xist showed enrichment across the entire X-chromosome (average enrichment = 23-fold), we observed differences in the precise levels of enrichment across the chromosome (Fig. 2A), which were highly reproducible between replicates (Pearson's correlation = 0.94, Fig. S4) (35). To characterize this variation, we correlated Xist enrichment with other genomic features (Table S1). We found that Xist enrichment strongly correlated with H3K27me3 across the entire chromosome (Pearson's correlation = 0.69, Fig. 2A-B), consistent with the known role for Xist in the recruitment of PRC2 (14, 22, 23). Xist levels also showed a strong correlation with gene density (Pearson's correlation = 0.44) and a negative correlation with the density of LINE repeats (Pearson's correlation = −0.25) which tend to reside in gene-poor regions.

To further explore this variation, we examined the most-enriched (>30-fold) and least-enriched (<15-fold) regions of the X-chromosome (Fig. 2C) (35). The most-enriched regions show higher H3K27me3 occupancy in MLFs (1.7-fold) and higher gene density (3-fold) than the chromosome average, consistent with the chromosome-wide correlations. The least enriched regions contained genes known to escape XCI (36). Consistent with their preferential positioning outside of the Xist domain (37, 38), escape genes displayed a ~50%

reduction in Xist occupancy compared to silenced X-chromosome genes, with the level of Xist enrichment roughly reflecting the previously reported ratio of expression from the inactive versus active X-chromosome (Pearson correlation = −0.66, Fig. 2D) (35)(39). Closer examination of Xist localization at some escape genes sometimes revealed sharp boundaries separating escaped and non-escaped domains (Fig. 2E). One of the least-enriched regions resided immediately distal to the Xist locus and included the lncRNA genes *Jpx* and *Ftx*, both of which have been previously reported to escape XCI and act as positive regulators of *Xist*(40, 41) (Fig. 2F).

Altogether, the least-enriched regions contain 53 genes with more than 40% depletion for Xist compared to the chromosome average (Table S2). Twenty-four of these genes have been previously reported to partially escape inactivation, including ten microRNA genes (42) and three lncRNAs (Table S2). Three of these genes represent novel candidate escape genes in MLF, displaying on average 50% depletion of Xist compared to other genes on the X-chromosome. The remaining genes are not expressed in MLF or are located within 300-Kb of a known escape gene and thus likely do not escape XCI in this cell type.

Thus, the Xist RNA localizes broadly across the entire inactive X-chromosome in differentiated cells, preferentially localizing at gene-rich regions (43, 44) but excluding genes that are expressed on the inactive X-chromosome. This broad localization pattern suggests that Xist localizes to chromatin in a degenerate fashion, possibly through interactions with the nuclear matrix (29, 30, 44).

Xist initially localizes to defined regions across the X-chromosome

To gain insights into how Xist establishes this broad localization pattern during the initiation of XCI, we examined Xist localization upon activation in mouse embryonic stem (ES) cells (20). In the pluripotent state, Xist is not expressed and both X-chromosomes are active (20, 21, 45, 46). Induction of differentiation triggers Xist activation on one allele, leading to the silencing of the X-chromosome in *cis*(20, 21, 45). To synchronize the initiation of XCI, we engineered a tetracycline-inducible promoter to drive Xist expression from its endogenous locus in a male mouse ES cell line (Fig. 3A, Fig. S5) (35). Upon induction with doxycycline, these cells increased Xist expression ~120-fold over a period of six hours (Fig. S6). RNA FISH showed that after one hour of induction Xist appeared as a strong focal point and grew to a characteristic cloud over time (Fig. 3B, Fig. S6), accompanied by exclusion of RNA polymerase II and accumulation of PRC2 and H3K27me3 over the Xist RNA compartment (Fig. S6). Cells expressing Xist concurrently silenced expression of the Tsix RNA, which negatively regulates Xist in ES cells (Fig. S6) (47).

To observe the process by which Xist initially spreads across the X-chromosome, we used RAP to generate high-resolution maps of Xist localization across 5 time points between zero and six hours after Xist induction (Fig. 3C, Fig. S7). After one hour of Xist induction, we observed a strong ~5-Mb peak centered at the Xist transcription locus, corresponding to the spot of Xist localization observed using RNA FISH (Fig. 3B, Fig. S6). Over the time-course, this peak declined while Xist levels across the chromosome increased. These patterns mirrored the emergence of the large Xist cloud observable by FISH at these time points. By six hours, the pattern of Xist localization began to resemble stable XCI in MLFs, where Xist localizes broadly across the X-chromosome and is preferentially enriched at gene-dense regions (Fig. S7).

Two models have been proposed to explain how Xist accomplishes this rapid spreading across the entire X-chromosome (Fig. 3D) (44, 48): either Xist spreads uniformly from its transcription site until it coats the entire chromosome, or Xist first localizes to “early” sites that are far from the Xist transcription locus (44). To distinguish between these models, we

examined Xist localization by RAP after one hour of Xist induction. We identified 28 distal sites of Xist occupancy across the chromosome ($P < 0.05$, Fig. 3E) (35). These sites comprised broad domains (average size 367 Kb) that were concentrated in 15 regions spaced across the entire X-chromosome. These sites initially showed an ~2-fold enrichment compared to neighboring regions, but this enrichment decreased over time (Fig. 3C), suggesting that Xist preferentially localizes to these sites early during the initiation of XCI. We also performed the RAP experiment across a differentiation time-course in wild-type female ES cells (Fig. S8) (35). We found that Xist localized to these same distal sites across the X-chromosome in female ES cells (Fig. 3F, Fig. S7, Fig. S9), demonstrating that Xist also targets these early sites in a normal developmental context. Thus, Xist initially transfers from its transcription locus to distal early localization sites to initiate spreading across the X-chromosome.

3-D chromosome conformation guides Xist to early localization sites

To determine how Xist identifies and targets these early localization sites, we considered two possible explanations (Fig. 4A). (i) Early sites may have higher affinity for the Xist RNA, enabling them to recruit Xist as it diffuses away from its transcription locus ('affinity transfer') (48-51). (ii) Alternatively, early sites may be defined not by affinity for Xist RNA but by spatial proximity to the site of Xist transcription ('proximity transfer') (44, 49).

We first explored the affinity transfer model. Early sites were not enriched for specific sequence motifs that could play a role in recruiting Xist (35). We further compared Xist enrichment to >250 genomic annotations, including features such as repeat element density and ChIP-Seq experiments in ES cells (Table S1) (35). We did not observe a significant relationship between Xist localization and LINE1 repeat elements (Pearson's correlation = −0.17) (supplementary online text). Instead, Xist early localization sites displayed modest enrichments (<2-fold) for gene density (Table S3). Yet, the chromosome-wide correlation between Xist localization and gene density was relatively modest (Pearson's correlation = 0.34) (35), suggesting that gene density alone does not explain early Xist localization patterns.

In the proximity transfer model (Fig. 4A) the early Xist localization sites would be in close spatial proximity to the *Xist* transcription locus *prior* to Xist RNA induction, allowing direct transfer upon transcription of Xist RNA from its genomic locus to linearly distant chromosomal regions. To test this hypothesis, we examined the conformation of the X-chromosome using a previously published male mouse ES cell dataset (52) generated by genome-wide chromosome conformation capture (Hi-C (53)). Because of the sparseness of the Hi-C contact maps, we binned the data into 1-Mb regions based on the distance from the *Xist* genomic locus (35). We found a strong correlation between Xist RNA localization across the X-chromosome and the frequency at which distal sites contact the *Xist* genomic locus (Pearson's correlation = 0.69, Fig. 4B). We note that this correlation is not driven by the strong peak in both datasets centered at the *Xist* genomic locus because we considered only sites further than 10 Mb from *Xist* itself (35). This strong correlation was also observed upon differentiation of female ES cells (Pearson's correlation = 0.69, Fig. S10A). These correlations exceeded that of any of the >250 genomic annotations that we tested in ES cells (Table S1).

One possible explanation for this correlation is that RAP might be capturing distal sites due to their proximity-mediated contacts with the *Xist* DNA locus, rather than due to interactions with the Xist RNA. This is possible because in Xist RAP the *Xist* DNA locus is enriched ~10-fold compared to the rest of the X-chromosome (Fig. 4B). By capturing the *Xist* DNA locus through purification of Xist RNA, we might indirectly enrich other distal sites that are crosslinked to the *Xist* DNA locus, thereby yielding a pattern of enrichment

similar to a standard chromosome conformation capture assay. However, if we observed a similar correlation between early Xist localization and chromosome conformation in the absence of a strong localization peak at the *Xist* genomic locus, then the pattern of Xist enrichment across the chromosome cannot be explained by proximity-induced crosslinking effects. To test this, we used our inducible system to turn off Xist transcription after one hour of induction and profiled Xist localization (35). We found that Xist RNA enrichment at its DNA locus declined from 102-fold to 14-fold over input, showing a level comparable to the rest of the X-chromosome (Fig. S10B). Xist remained enriched at the same distal regions (Fig. S7, Fig. S9) and showed a comparable correlation with proximity contacts to the *Xist* DNA locus (Pearson's correlation = 0.59, Fig. S10C), arguing that the Xist RNA interacts directly with these spatially proximal sites.

These data demonstrate that early Xist localization correlates with spatial proximity, but do not demonstrate a causal relationship between Xist localization and chromosome conformation. If initial Xist localization is controlled by proximity-mediated contact with the *Xist* genomic locus, then altering the conformational context of the *Xist* transcription locus should lead to an early localization pattern defined by the proximity contacts of the new integration site. To test this directly, we utilized a male ES cell line that expresses an Xist cDNA from a Tet-inducible transgene incorporated at the *Hprt* locus, a genomic locus ~50 Mb proximal to the endogenous *Xist* locus (26) (Fig. S7, Fig. S10D). When we examined these cells at early time points after induction, we found that early Xist localization correlated strongly with proximity contacts at the *Hprt* integration site (Pearson's correlation = 0.92, Fig. 4C) but not with those at the endogenous *Xist* locus (Pearson's correlation = −0.02). While these results do not exclude the possibility that additional chromatin features may be important for creating a permissive environment for Xist RNA localization, it is clear that chromosome conformation plays a dominant role in determining the early localization sites of the Xist RNA on the X-chromosome.

Thus, spatial proximity to the Xist transcription locus guides early Xist RNA localization. This proximity-guided search may explain several of our other observations about Xist localization. (i) Because Xist is actively transcribed, it will be located within the ‘active compartment’ of the nucleus (53). This may explain our observations that Xist preferentially localizes to gene-rich regions. (ii) Because chromosome conformation is heterogeneous in a cell population (54, 55), the precise order by which Xist spreads to distal sites is likely to differ between individual cells. This may explain why Xist shows low-level early enrichment across the entire X-chromosome as all regions of the chromosome may contact the *Xist* genomic locus at some low frequency.

Xist spreading to active genes depends on its silencing domain

Although early Xist localization correlated strongly with proximity contact frequency across the chromosome, we noticed several large chromosomal domains where Xist occupancy was lower than would be expected based on the observed proximity contacts (*e.g.*, black arrows in Fig. 4B). These depleted regions contained many genes that are actively transcribed in ES cells; we termed these “active gene-dense regions”. In contrast, the early-enriched Xist localization sites were also gene-dense but were enriched for genes that are *inactive* in ES cells. The depleted regions neighbored the early Xist localization sites such that Xist accumulated on the periphery of active gene-dense regions (Fig. S11A).

To test whether actively transcribed genes generally showed reduced Xist occupancy, we explored Xist localization across all genes on the X-chromosome three hours after Xist induction. Indeed, Xist showed on average a 15% focal depletion over active genes (P = 0.006, Mann-Whitney test), but was not depleted across inactive genes (Fig. 5A,B). The level of Xist occupancy across active genes roughly reflected the level of expression in ES

cells, with highly transcribed genes showing the lowest Xist occupancy (Pearson's correlation = -0.33, Fig. S11B). Furthermore, this focal depletion across active genes was temporary: Xist enrichment at genes expressed in ES cells increased over time and upon stable inactivation in MLFs was comparable to neighboring intergenic regions and inactive genes (Fig. S11C). Together, these results suggest that the initial localization of Xist is hindered by some feature of actively transcribed genes but that Xist can eventually overcome this barrier to spread across these regions.

We hypothesized that the ability of Xist to spread across active genes is dependent on its ability to silence gene expression. Previous genetic studies have identified the A-repeat within Xist as an RNA domain that is necessary for silencing gene expression but that is not required for the formation of the Xist RNA compartment (25, 26). We therefore repeated the RAP experiments using an Xist RNA in which the A-repeat had been deleted (ΔA Xist) (26). We found that the localization of ΔA Xist over the whole X-chromosome looked broadly comparable to that of wild-type Xist (Fig. 5C, Fig. S12), consistent with previous observations by FISH (25, 26). However, at high resolution, we observed a ~2-fold depletion for ΔA Xist occupancy compared to wild-type Xist over active gene-dense regions, with ΔA Xist instead accumulating on the edges of these regions (Fig. 5C, Fig. S11D,E). This depletion extended across the entire region including active and inactive genes as well as intergenic sequences, suggesting that active gene-dense regions may loop out of the ΔA Xist compartment such that even inactive genes remain physically inaccessible to ΔA Xist spreading (Fig. 5E).

These results demonstrate that Xist initially localizes to the periphery of active gene-dense regions through a mechanism independent of its A-repeat domain, but requires the A-repeat to efficiently spread across active genes and access these regions. Notably, the A-repeat domain interacts with the PRC2 chromatin-modifying complex (14) and enables the spatial repositioning of active genes into the Xist compartment (25). Together, these observations suggest that the A-repeat may allow Xist to access and spread across active gene-dense regions by modifying chromatin and altering chromosome architecture to reposition these regions into the Xist compartment (Fig. 5E).

A model for how Xist exploits and alters three-dimensional genome architecture to spread across the X-chromosome

Our data suggest a model for how Xist can integrate its two functions – localization to DNA and silencing of gene expression – to exploit and alter nuclear architecture to spread across the X-chromosome (Fig. 6). In this model, at the initiation XCI, Xist exploits the pre-existing three-dimensional conformation of the X-chromosome to search for target sites across the chromosome. Upon encountering a new site, Xist transfers to this region through a mechanism that allows it to localize to any region of the X-chromosome, possibly through its interaction with proteins in the nuclear matrix (29-31). Initially, Xist accumulates at spatially proximal sites on the periphery of active gene-dense regions, positioning itself to silence neighboring genes. Through the A-repeat domain, Xist leads to transcriptional silencing (26) and repositioning of these genes into the growing Xist silenced compartment (25), possibly through recruitment of PRC2 (14) and other proteins (56) that lead to chromosomal compaction (57, 58). By repositioning previously active regions into its growing compartment, Xist effectively pulls new regions of active chromatin closer to the *Xist* transcription locus, thus allowing Xist RNA to spread to new sites by proximity transfer. Since Xist is actively transcribed throughout XCI, it will remain spatially close to other actively transcribed genes (59) – the precise targets required for propagating Xist-mediated silencing. This process – involving searching in three dimensions, modifying chromatin state and chromosome architecture, and spreading to newly accessible locations – would explain how Xist can silence the entire X-chromosome reproducibly, such that

silencing occurs in each cell, despite the fact that chromosome conformation and thus the early Xist localization sites may vary between individual cells in a population.

This coordinated interplay between lncRNA localization and chromosome conformation may have broader implications beyond Xist. Other lncRNAs may similarly take advantage of chromosome conformation to identify target sites in close spatial proximity (9, 17, 60), which could even reside on other chromosomes (61, 62). This search strategy capitalizes on the ability of a lncRNA to act while tethered to its transcription locus (63), in contrast to an mRNA which requires export and translation to carry out its function. Because chromosome conformation is nonrandom, a proximity-guided search strategy might explain how low-abundance lncRNAs can reliably identify their genomic targets. Upon binding these targets, lncRNAs may in turn alter chromosome conformation through their interactions with various chromatin regulatory complexes (15, 16). These alterations would allow localization to and regulation of previously inaccessible chromatin domains, and might even establish local nuclear compartments that contain the co-regulated targets of lncRNA complexes.

Methods

RNA Antisense Purification (RAP)

We designed a set of 120-nucleotide oligos tiled every 15 nucleotides across the entire Xist RNA sequence, excluding sequences that originated from a repetitive region. We synthesized this pool of oligos using microarray-based DNA synthesis technology and incorporated T7 promoter sequences through PCR. We generated RNA probes by *in vitro* transcription in the presence biotin-UTP. We crosslinked cells with 2 mM disuccinimidyl glutarate for 45 minutes and 3% formaldehyde for 10 minutes. We lysed cells and digested chromatin to 100-300 bp fragments through a combination of sonication and treatment with TURBO DNase. We diluted the lysate to hybridization conditions containing 3 M guanidine thiocyanate. We precleared lysate preparations by adding streptavidin-coated magnetic beads for 20 minutes at 45°C. Biotin-labeled RNA capture probes were mixed with the heated lysate and incubated at 45°C for 2 hours. We captured the probe-RNA complexes with streptavidin-coated beads and washed six times at 45°C. We eluted captured chromatin complexes and reversed crosslinks by adding Proteinase K to the probe-bead complexes and incubating overnight at 65°C. We generated standard Illumina sequencing libraries and obtained >5 million 25-bp paired-end reads per sample.

Inducible Xist cell lines

For the time-course, we used a male ES cell line in which the wild-type *Xist* promoter was replaced with a Tet-inducible promoter. For chromosome conformation and A-repeat deletion experiments, we used male ES cell lines carrying a wild-type or ΔA Xist cDNA transgene in the *Hprt* locus under control of a Tet-inducible promoter. To induce Xist expression, we added doxycycline to a final concentration of 2 μg/mL at a defined time before fixing cells.

Data analysis

Sequencing reads were aligned to the *Mus musculus* genome (mm9). We calculated enrichment ratios between read counts in the RAP experiment and the input in overlapping windows across the chromosome. To identify early sites in the time-course experiments, we looked for 100-Kb windows with enrichments that exceeded the local mean ($P < 0.05$). We correlated Xist enrichment across the chromosome with normalized Hi-C interaction counts measured in male mouse ES cells at 1-Mb resolution (52). For Hi-C correlation analysis, we excluded all bins within 10 Mb on either side of the *Xist* transcription locus, which would otherwise dominate the correlation calculation due to the strong local peaks in both the Hi-C

and RAP datasets. To define active and inactive genes, we analyzed RNA-Seq data from embryonic stem cells and defined “active” genes as those expressed with $P < 0.001$.

Complete materials and methods are available as supplementary material.

Supplementary Material

Refer to Web version on PubMed Central for supplementary material.

Acknowledgments

We thank Andi Gnirke for initial discussions about the RAP method; Tarjei Mikkelsen for assistance with oligonucleotide synthesis; Manuel Garber and John Rinn for helpful discussions and ideas; Anton Wutz for generously providing Xist transgenic cell lines; Suhas Rao, Neva Cherniavsky, and Erez Lieberman-Aiden for analytical help and discussions; Pam Russell, Moran Cabili, Ezgi Hacisuleyman, and Loyal Goff for critical reading of the manuscript; Leslie Gaffney for assistance with figures; and Sigrid Knemeyer for illustrations. JE is supported by the Fannie and John Hertz Foundation and NDSEG Fellowships. APJ is supported by an NIH post-doctoral fellowship (1F32GM103139-01). This work was funded by an NIH Director's Early Independence Award (DP5OD012190 to MG), NHGRI Center for Excellence for Genomic Sciences (P50HG006193 to MG), NIGMS (P01GM099134 to KP), CIRM (RN1-00564, RB3-05080, and RB4-06133 to KP), and funds from the Broad Institute of MIT and Harvard (MG and ESL) and the Eli and Edythe Broad Center of Regenerative Medicine and Stem Cell Research at UCLA (KP). JE, ESL, and MG are inventors on a provisional patent on the RAP method. Sequencing data is available online from the NCBI Gene Expression Omnibus (accession GSE46918, http://www.ncbi.nlm.nih.gov/geo/) and additional data and information is available at www.lncRNA.caltech.edu/RAP/.

References

1. Derrien T, et al. The GENCODE v7 catalog of human long noncoding RNAs: analysis of their gene structure, evolution, and expression. Genome Res. Sep.2012 22:1775. [PubMed: 22955988]
2. Carninci P, et al. The transcriptional landscape of the mammalian genome. Science. Sep 2.2005 309:1559. [PubMed: 16141072]
3. Guttman M, et al. Ab initio reconstruction of cell type-specific transcriptomes in mouse reveals the conserved multi-exonic structure of lincRNAs. Nat Biotechnol. May.2010 28:503. [PubMed: 20436462]
4. Guttman M, et al. Chromatin signature reveals over a thousand highly conserved large non-coding RNAs in mammals. Nature. Mar 12.2009 458:223. [PubMed: 19182780]
5. Cabili MN, et al. Integrative annotation of human large intergenic noncoding RNAs reveals global properties and specific subclasses. Genes Dev. Sep 15.2011 25:1915. [PubMed: 21890647]
6. Guttman M, et al. lincRNAs act in the circuitry controlling pluripotency and differentiation. Nature. Sep 15.2011 477:295. [PubMed: 21874018]
7. Ulitsky I, Shkumatava A, Jan CH, Sive H, Bartel DP. Conserved function of lincRNAs in vertebrate embryonic development despite rapid sequence evolution. Cell. Dec 23.2011 147:1537. [PubMed: 22196729]
8. Orom UA, et al. Long noncoding RNAs with enhancer-like function in human cells. Cell. Oct 1.2010 143:46. [PubMed: 20887892]
9. Wang KC, et al. A long noncoding RNA maintains active chromatin to coordinate homeotic gene expression. Nature. Apr 7.2011 472:120. [PubMed: 21423168]
10. Rinn JL, et al. Functional demarcation of active and silent chromatin domains in human HOX loci by noncoding RNAs. Cell. Jun 29.2007 129:1311. [PubMed: 17604720]
11. Lee JT. Epigenetic regulation by long noncoding RNAs. Science. Dec 14.2012 338:1435. [PubMed: 23239728]
12. Tsai MC, et al. Long noncoding RNA as modular scaffold of histone modification complexes. Science. Aug 6.2010 329:689. [PubMed: 20616235]
13. Nagano T, et al. The Air noncoding RNA epigenetically silences transcription by targeting G9a to chromatin. Science. Dec 12.2008 322:1717. [PubMed: 18988810]

14. Zhao J, Sun BK, Erwin JA, Song JJ, Lee JT. Polycomb proteins targeted by a short repeat RNA to the mouse X chromosome. Science. Oct 31.2008 322:750. [PubMed: 18974356]
15. Guttman M, Rinn JL. Modular regulatory principles of large non-coding RNAs. Nature. Feb 16.2012 482:339. [PubMed: 22337053]
16. Rinn JL, Chang HY. Genome regulation by long noncoding RNAs. Annu Rev Biochem. 2012; 81:145. [PubMed: 22663078]
17. Kanhere A, Jenner RG. Noncoding RNA localisation mechanisms in chromatin regulation. Silence. 2012; 3:2. [PubMed: 22292981]
18. Gontan C, Jonkers I, Gribnau J. Long Noncoding RNAs and X Chromosome Inactivation. Prog Mol Subcell Biol. 2011; 51:43. [PubMed: 21287133]
19. Umlauf D, Fraser P, Nagano T. The role of long non-coding RNAs in chromatin structure and gene regulation: variations on a theme. Biol Chem. Apr.2008 389:323. [PubMed: 18225988]
20. Plath K, Mlynarczyk-Evans S, Nusinow DA, Panning B. Xist RNA and the mechanism of X chromosome inactivation. Annu Rev Genet. 2002; 36:233. [PubMed: 12429693]
21. Avner P, Heard E. X-chromosome inactivation: counting, choice and initiation. Nat Rev Genet. Jan.2001 2:59. [PubMed: 11253071]
22. Plath K, et al. Role of histone H3 lysine 27 methylation in X inactivation. Science. Apr 4.2003 300:131. [PubMed: 12649488]
23. Silva J, et al. Establishment of histone h3 methylation on the inactive X chromosome requires transient recruitment of Eed-Enx1 polycomb group complexes. Dev Cell. Apr.2003 4:481. [PubMed: 12689588]
24. Clemson CM, McNeil JA, Willard HF, Lawrence JB. XIST RNA paints the inactive X chromosome at interphase: evidence for a novel RNA involved in nuclear/chromosome structure. J Cell Biol. Feb.1996 132:259. [PubMed: 8636206]
25. Chaumeil J, Le Baccon P, Wutz A, Heard E. A novel role for Xist RNA in the formation of a repressive nuclear compartment into which genes are recruited when silenced. Genes Dev. Aug 15.2006 20:2223. [PubMed: 16912274]
26. Wutz A, Rasmussen TP, Jaenisch R. Chromosomal silencing and localization are mediated by different domains of Xist RNA. Nat Genet. Feb.2002 30:167. [PubMed: 11780141]
27. Senner CE, et al. Disruption of a conserved region of Xist exon 1 impairs Xist RNA localisation and X-linked gene silencing during random and imprinted X chromosome inactivation. Development. Apr.2011 138:1541. [PubMed: 21389056]
28. Beletskii A, Hong YK, Pehrson J, Egholm M, Strauss WM. PNA interference mapping demonstrates functional domains in the noncoding RNA Xist. Proc Natl Acad Sci U S A. Jul 31.2001 98:9215. [PubMed: 11481485]
29. Hasegawa Y, Brockdorff N, Kawano S, Tsutui K, Nakagawa S. The matrix protein hnRNP U is required for chromosomal localization of Xist RNA. Dev Cell. Sep 14.2010 19:469. [PubMed: 20833368]
30. Pullirsch D, et al. The Trithorax group protein Ash2l and Saf-A are recruited to the inactive X chromosome at the onset of stable X inactivation. Development. Mar.2010 137:935. [PubMed: 20150277]
31. Agrelo R, et al. SATB1 defines the developmental context for gene silencing by Xist in lymphoma and embryonic cells. Dev Cell. Apr.2009 16:507. [PubMed: 19386260]
32. Chu C, Qu K, Zhong FL, Artandi SE, Chang HY. Genomic maps of long noncoding RNA occupancy reveal principles of RNA-chromatin interactions. Mol Cell. Nov 18.2011 44:667. [PubMed: 21963238]
33. Simon MD, et al. The genomic binding sites of a noncoding RNA. Proc Natl Acad Sci U S A. Dec 20.2011 108:20497. [PubMed: 22143764]
34. Mariner PD, et al. Human Alu RNA is a modular transacting repressor of mRNA transcription during heat shock. Mol Cell. Feb 29.2008 29:499. [PubMed: 18313387]
35. Materials and methods are available as supplementary material on *Science* Online.
36. Berletch JB, Yang F, Xu J, Carrel L, Disteche CM. Genes that escape from X inactivation. Hum Genet. Aug.2011 130:237. [PubMed: 21614513]

37. Dietzel S, et al. The 3D positioning of ANT2 and ANT3 genes within female X chromosome territories correlates with gene activity. Exp Cell Res. Nov 1.1999 252:363. [PubMed: 10527626]
38. Filippova GN, et al. Boundaries between chromosomal domains of X inactivation and escape bind CTCF and lack CpG methylation during early development. Dev Cell. Jan.2005 8:31. [PubMed: 15669143]
39. Yang F, Babak T, Shendure J, Disteche CM. Global survey of escape from X inactivation by RNA-sequencing in mouse. Genome Res. May.2010 20:614. [PubMed: 20363980]
40. Tian D, Sun S, Lee JT. The long noncoding RNA, Jpx, is a molecular switch for X chromosome inactivation. Cell. Oct 29.2010 143:390. [PubMed: 21029862]
41. Chureau C, et al. Ftx is a non-coding RNA which affects Xist expression and chromatin structure within the X-inactivation center region. Human molecular genetics. Feb 15.2011 20:705. [PubMed: 21118898]
42. Song R, et al. Many X-linked microRNAs escape meiotic sex chromosome inactivation. Nat Genet. Apr.2009 41:488. [PubMed: 19305411]
43. Duthie SM, et al. Xist RNA exhibits a banded localization on the inactive X chromosome and is excluded from autosomal material in cis. Human molecular genetics. Feb.1999 8:195. [PubMed: 9931327]
44. Tattermusch A, Brockdorff N. A scaffold for X chromosome inactivation. Hum Genet. Aug.2011 130:247. [PubMed: 21660507]
45. Arthold S, Kurowski A, Wutz A. Mechanistic insights into chromosome-wide silencing in X inactivation. Hum Genet. Aug.2011 130:295. [PubMed: 21567178]
46. Kim DH, Jeon Y, Anguera MC, Lee JT. X-chromosome epigenetic reprogramming in pluripotent stem cells via noncoding genes. Semin Cell Dev Biol. Jun.2011 22:336. [PubMed: 21376830]
47. Lee JT, Lu N. Targeted mutagenesis of Tsix leads to nonrandom X inactivation. Cell. Oct 1.1999 99:47. [PubMed: 10520993]
48. Pinter SF, et al. Spreading of X chromosome inactivation via a hierarchy of defined Polycomb stations. Genome Res. Oct.2012 22:1864. [PubMed: 22948768]
49. Marks H, et al. High-resolution analysis of epigenetic changes associated with X inactivation. Genome Res. Aug.2009 19:1361. [PubMed: 19581487]
50. Jeon Y, Lee JT. YY1 tethers Xist RNA to the inactive X nucleation center. Cell. Jul 8.2011 146:119. [PubMed: 21729784]
51. Heard E, et al. Methylation of histone H3 at Lys-9 is an early mark on the X chromosome during X inactivation. Cell. Dec 14.2001 107:727. [PubMed: 11747809]
52. Dixon JR, et al. Topological domains in mammalian genomes identified by analysis of chromatin interactions. Nature. May 17.2012 485:376. [PubMed: 22495300]
53. Lieberman-Aiden E, et al. Comprehensive mapping of long-range interactions reveals folding principles of the human genome. Science. Oct 9.2009 326:289. [PubMed: 19815776]
54. Dekker J, Marti-Renom MA, Mirny LA. Exploring the three-dimensional organization of genomes: interpreting chromatin interaction data. Nat Rev Genet. Jun.2013 14:390. [PubMed: 23657480]
55. Misteli T. The concept of self-organization in cellular architecture. J Cell Biol. Oct 15.2001 155:181. [PubMed: 11604416]
56. Nozawa RS, et al. Human inactive X chromosome is compacted through a PRC2-independent SMCHD1-HBiX1 pathway. Nature structural & molecular biology. May.2013 20:566.
57. Rego A, Sinclair PB, Tao W, Kireev I, Belmont AS. The facultative heterochromatin of the inactive X chromosome has a distinctive condensed ultrastructure. J Cell Sci. Apr 1.2008 121:1119. [PubMed: 18334550]
58. Naughton C, Sproul D, Hamilton C, Gilbert N. Analysis of active and inactive X chromosome architecture reveals the independent organization of 30 nm and large-scale chromatin structures. Mol Cell. Nov 12.2010 40:397. [PubMed: 21070966]
59. Splinter E, et al. The inactive X chromosome adopts a unique three-dimensional conformation that is dependent on Xist RNA. Genes Dev. Jul 1.2011 25:1371. [PubMed: 21690198]
60. Maass PG, et al. A misplaced lncRNA causes brachydactyly in humans. J Clin Invest. Nov 1.2012 122:3990. [PubMed: 23093776]

61. Williams A, Spilianakis CG, Flavell RA. Interchromosomal association and gene regulation in trans. Trends Genet. Apr.2010 26:188. [PubMed: 20236724]
62. Spilianakis CG, Lalioti MD, Town T, Lee GR, Flavell RA. Interchromosomal associations between alternatively expressed loci. Nature. Jun 2.2005 435:637. [PubMed: 15880101]
63. Lee JT. Lessons from X-chromosome inactivation: long ncRNA as guides and tethers to the epigenome. Genes Dev. Aug 15.2009 23:1831. [PubMed: 19684108]
64. Thompson J, Gillespie D. Molecular hybridization with RNA probes in concentrated solutions of guanidine thiocyanate. Anal Biochem. Jun.1987 163:281. [PubMed: 2444134]
65. Mili S, Steitz JA. Evidence for reassociation of RNA-binding proteins after cell lysis: implications for the interpretation of immunoprecipitation analyses. RNA. Nov.2004 10:1692. [PubMed: 15388877]
66. Tang YA, et al. Efficiency of Xist-mediated silencing on autosomes is linked to chromosomal domain organisation. Epigenetics Chromatin. 2010; 3:10. [PubMed: 20459652]
67. Gartler SM, Riggs AD. Mammalian X-chromosome inactivation. Annu Rev Genet. 1983; 17:155. [PubMed: 6364959]
68. Lyon MF. X-chromosome inactivation: a repeat hypothesis. Cytogenet Cell Genet. 1998; 80:133. [PubMed: 9678347]
69. Chow JC, et al. LINE-1 activity in facultative heterochromatin formation during X chromosome inactivation. Cell. Jun 11.2010 141:956. [PubMed: 20550932]
70. Versteeg R, et al. The human transcriptome map reveals extremes in gene density, intron length, GC content, and repeat pattern for domains of highly and weakly expressed genes. Genome Res. Sep.2003 13:1998. [PubMed: 12915492]
71. Panning B, Dausman J, Jaenisch R. X chromosome inactivation is mediated by Xist RNA stabilization. Cell. Sep 5.1997 90:907. [PubMed: 9298902]
72. LeProust EM, et al. Synthesis of high-quality libraries of long (150mer) oligonucleotides by a novel depurination controlled process. Nucleic Acids Res. May.2010 38:2522. [PubMed: 20308161]
73. Li H, Durbin R. Fast and accurate short read alignment with Burrows-Wheeler transform. Bioinformatics. Jul 15.2009 25:1754. [PubMed: 19451168]
74. Machanick P, Bailey TL. MEME-ChIP: motif analysis of large DNA datasets. Bioinformatics. Jun 15.2011 27:1696. [PubMed: 21486936]
75. Mendenhall EM, et al. GC-rich sequence elements recruit PRC2 in mammalian ES cells. PLoS Genet. 2010; 6:e1001244. [PubMed: 21170310]
76. A user's guide to the encyclopedia of DNA elements (ENCODE). PLoS Biol. Apr.2011 9:e1001046. [PubMed: 21526222]
77. Jurka J, et al. Repbase Update, a database of eukaryotic repetitive elements. Cytogenetic and genome research. 2005; 110:462. [PubMed: 16093699]
78. Helaers R, et al. gViz, a novel tool for the visualization of co-expression networks. BMC Res Notes. 2011; 4:452. [PubMed: 22032859]
79. Pontier DB, Gribnau J. Xist regulation and function explored. Hum Genet. Aug.2011 130:223. [PubMed: 21626138]

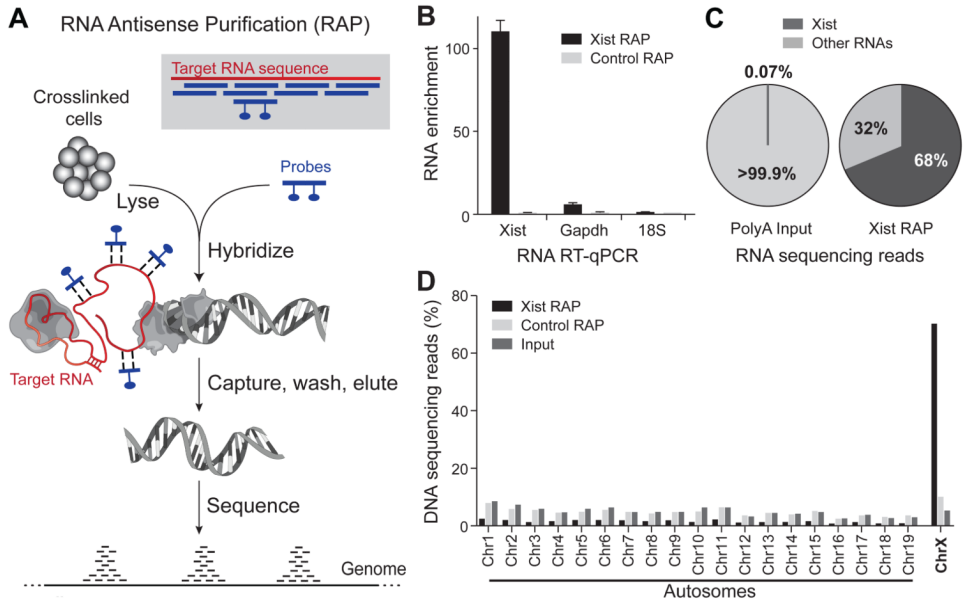

Fig. 1. RNA Antisense Purification accurately purifies lncRNA-chromatin interactions

(A) Schematic diagram of RAP. Biotinylated probes (blue) are hybridized to the target RNA (red) crosslinked to proteins and DNA. Gray inset: 120-mer antisense capture probes are designed to tile across the entire target RNA. **(B)** RT-qPCR of the RNA captured using antisense probes to Xist (Xist RAP, black) or sense probes to Xist (Control RAP, gray) in MLFs. Enrichments represent mean +/− SEM ($N = 3$ replicate experiments) and are normalized to the mean of the sense control experiments. We note that Tsix, an antisense transcript overlapping Xist, is not expressed in MLFs. **(C)** RNA sequencing reads originating from the Xist transcript (dark gray) and all other cellular RNAs (light gray) for polyA-selected RNA (left) and RNA captured using antisense probes for the Xist RNA (right) (35). **(D)** DNA sequencing reads aligning to each chromosome after purification with antisense probes (Xist RAP, black) and sense probes (Control RAP, light gray), and input genomic DNA (dark gray) in MLFs.

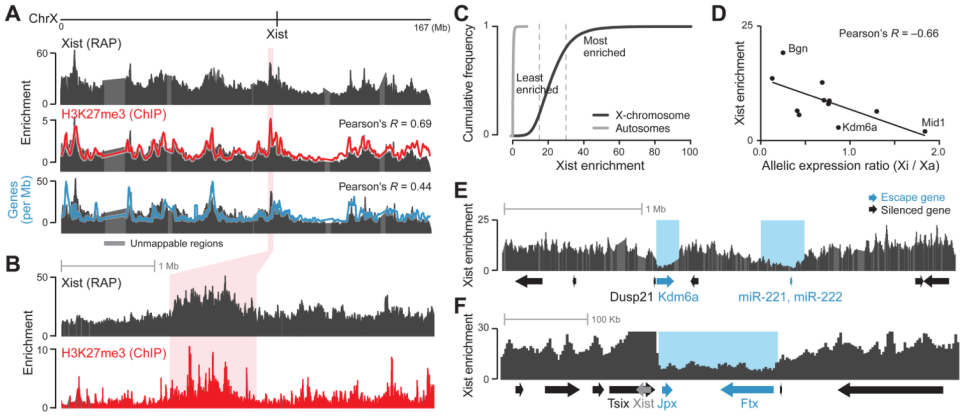

Fig. 2. High-resolution mapping of Xist localization on the inactive X-chromosome in differentiated female cells

(A) Xist enrichment over input (dark gray), H3K27me3 enrichment over input (red line), and gene density (blue line) (35) across the entire X-chromosome in female MLFs. **(B)** Zoom in on a highly-enriched Xist region (light-red box, chrX:95,000,000-99,000,000) shows Xist (black) and H3K27me3 (red) enrichments. **(C)** Cumulative distribution plot comparing Xist enrichment across all 10-Kb windows on the X-chromosome (black) and on autosomes (gray). Dashed lines demarcate the least- and most-highly enriched regions on the X-chromosome. **(D)** Correlation between Xist enrichment and the ratio of expression from the inactive X (Xi) and active X (Xa) for known escape genes (39). **(E)** Xist enrichment (chrX:17,031,000-19,901,000) across two of the least-enriched regions (blue boxes). **(F)** Xist enrichment around the *Xist* genomic locus including a least-enriched region (blue box). Xist enrichment at the *Xist* locus (gray arrow) extends above the *y*-axis maximum.

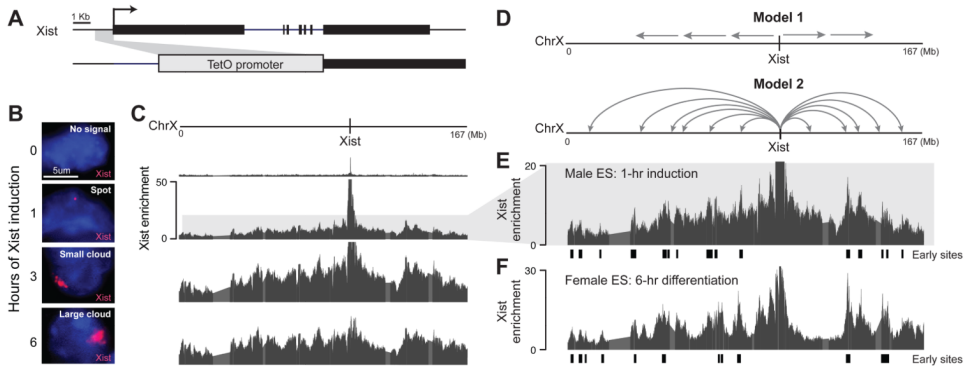

Fig. 3. High-resolution view of Xist spreading during initiation of XCI

(A) We replaced the 1,027 bases upstream of Xist with a tetracycline-responsive (TetO) promoter in male mouse ES cells (35). **(B)** Representative FISH images for the Xist RNA (red) and DAPI staining of the nucleus (blue) after Xist induction with doxycycline. Xist FISH signals were classified into categories – including no signal, spot, small cloud, and large cloud – at each time point (35). **(C)** Xist RAP enrichments over input across the X-chromosome for the same time points as in (B). The *y*-axis scale (0-50) is the same for all time points. Xist enrichment at the *Xist* locus extends above *y*-axis maximum. **(D)** Two proposed models for Xist spreading (gray arrows) from its transcription locus (tick mark) across the chromosome. **(E)** A zoom in on the *y*-axis of Xist enrichment after one hour of Xist induction. **(F)** Xist enrichments from RAP in wild-type female ES cells after 6 hours of differentiation. Early sites are defined by significant deviations ($P < 0.05$) above the local (10-Mb) average (35).

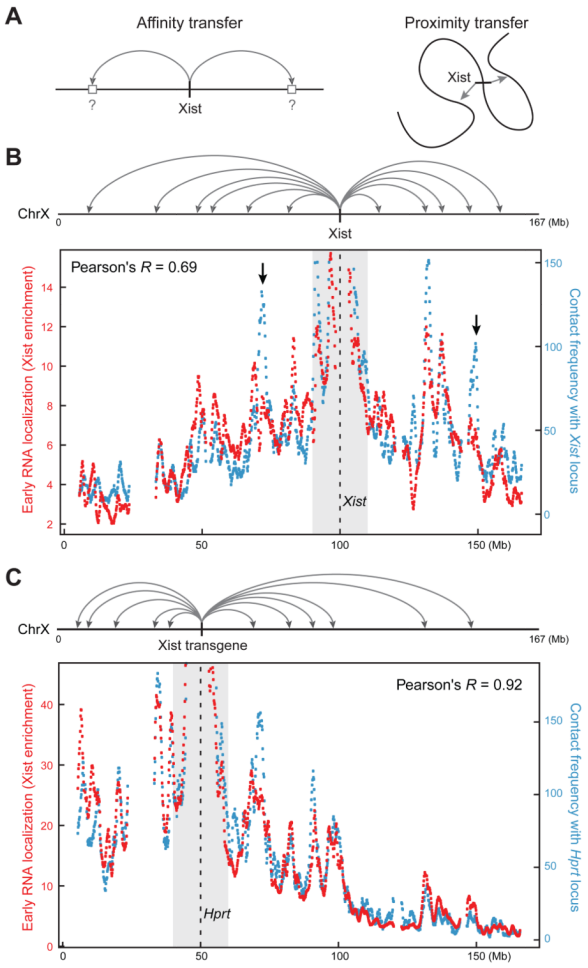

Fig. 4. Early Xist localization correlates with the 3-D proximity contacts of the Xist transcription locus

(A) Two models for how Xist spreads to early initiation sites (marked by gray arrows in all panels). Gray boxes on the left model represent hypothetical high-affinity interaction sites. **(B)** Correlation between Xist RNA localization (red) after one hour of Xist induction and Hi-C contact frequencies (blue) between distal sites and the *Xist* genomic locus (dashed line). Black arrows point to selected regions with lower Xist RNA enrichments than would be expected from the Hi-C contact frequencies. **(C)** Correlation between Xist transgene RNA localization (red) after three hours of induction of the Xist cDNA transgene in the *Hprt* locus and Hi-C contact frequencies (blue) between distal sites and the *Hprt* integration locus (dashed line). Correlation calculations exclude the shaded gray regions (10-Mb on each side). Contact frequencies represent normalized Hi-C interaction counts in male ES cells between each window and the window containing the *Xist* or *Hprt* locus (35).

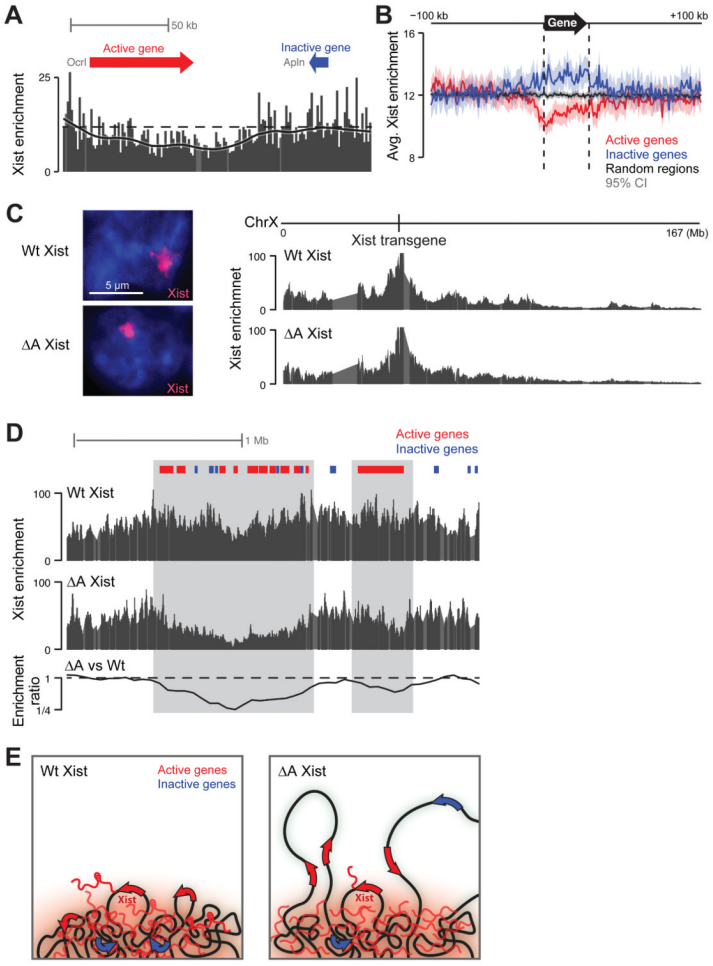

Fig. 5. The A-repeat deletion of Xist cannot spread over the active regions of the X-chromosome

(A) Xist enrichment over representative genes at chrX:45,252,000-45,408,000. Dashed line denotes the average enrichment for the entire region. Solid line represents the smoothed enrichment in sliding windows across the region. **(B)** Xist enrichment averaged over all active genes (red line, $N = 608$), inactive genes (blue line, $N = 595$), and randomly permuted regions across the X-chromosome (black line) (35). Shaded regions represent 95% confidence intervals for the average enrichment. **(C)** Localization of wild-type Xist (wt Xist, top) and Xist lacking the A-repeat (ΔA Xist, bottom) by RNA FISH (left) and RAP (right) across the X-chromosome. **(D)** Comparison of wt and ΔA Xist enrichment across a representative region at chrX:44,600,000-47,100,000. Gray boxes mark regions that are depleted for Xist localization in ΔA versus wt Xist. All panels present data from three hours after Xist induction in undifferentiated male ES cells, where Xist is expressed from its endogenous locus **(A-B)** or from the *Hprt* locus **(C-D)**. Genes were classified as active or inactive using RNA-Seq data from undifferentiated male ES cells (35). **(D)** Model: in the presence of the A-repeat (left), Xist localizes across the entire X-chromosome (red cloud) but is initially excluded from active genes (red arrows). In the absence of the A-repeat (right), Xist accumulates on the periphery of active gene-dense regions but cannot spread to actively transcribed genes (red arrows) or inactive genes (blue arrows) that lie within these regions.

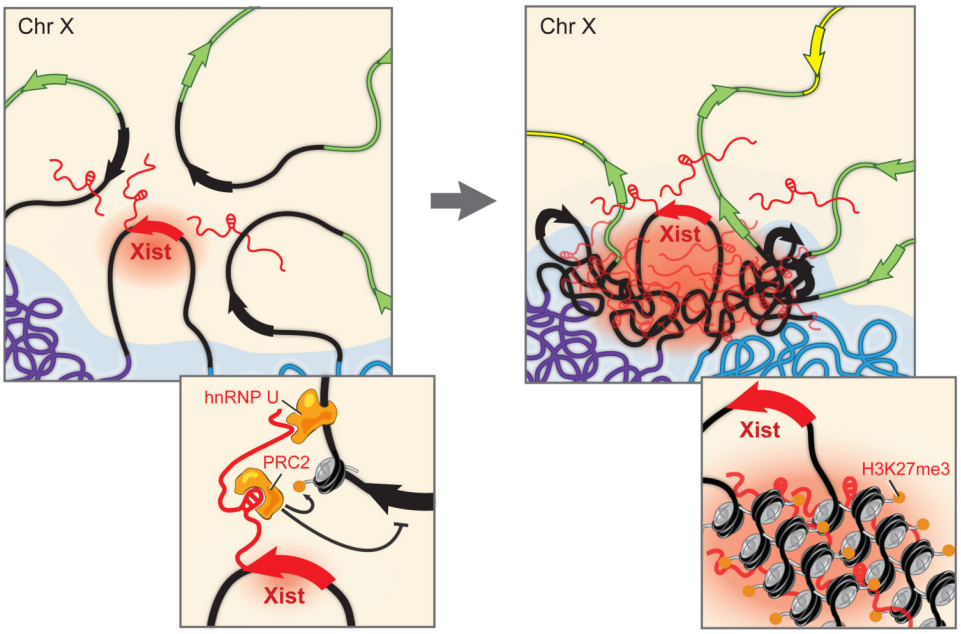

Fig. 6. A model for how Xist exploits and alters three-dimensional genome architecture to spread across the X-chromosome

Upon induction of expression in ES cells (left), Xist (red) spreads to spatially proximal sites on the periphery of active gene-dense regions (black). Gene-poor regions (blue, purple) contact the *Xist* transcription locus infrequently, leading to slower spreading to these regions. When encountering a new region (left inset), Xist interacts with chromatin through a degenerate localization mechanism, possibly through the matrix protein hnRNP U (30, 34), and uses its A-repeat domain to spread over active genes. Xist may then recruit PRC2 (14) and other proteins (56) to modify and compact chromatin, thereby repositioning nearby chromosomal regions into the Xist RNA compartment (red cloud, right inset). These structural changes may propagate Xist spreading (right) by pulling new regions (green, yellow) of the chromosome into closer proximity to the *Xist* genomic locus and the growing Xist compartment.